

Thermoelectric properties and texture evaluation of $\text{Ca}_3\text{Co}_4\text{O}_9$ prepared by a cost-effective multisheet cofiring technique

O-Jong Kwon · Wook Jo · Kyeong-Eun Ko ·
Jae-Yeol Kim · Sung-Hwan Bae · Hyun Koo ·
Seong-Min Jeong · Jin-Sang Kim · Chan Park

Received: 3 September 2010 / Accepted: 6 December 2010 / Published online: 16 December 2010
© Springer Science+Business Media, LLC 2010

Abstract Highly textured $\text{Ca}_3\text{Co}_4\text{O}_9$ thermoelectrics were fabricated by a so-called multisheet cofiring (MSC) technique in combination with the commonly practiced spark plasma sintering (SPS) technique. X-ray diffraction analysis revealed that the MSC technique significantly enhances the degree of texture compared with the conventional SPS technique. This was confirmed by microstructure analysis performed on polished and chemically etched specimens. The power factor and the thermoelectric figure of merit for the specimen produced by the MSC technique were estimated to be $\sim 5.2 \times 10^{-4} \text{ W/mK}^2$ and ~ 0.4 , respectively, both of which are $\sim 20\%$ larger than those of the normally processed specimens. A comparative study of the thermoelectric properties, such as electrical resistivity and Seebeck coefficient, clearly demonstrated that texture mainly influences the electrical resistivity and consequently enhances the thermoelectric properties.

O.-J. Kwon · K.-E. Ko · J.-Y. Kim · S.-H. Bae · H. Koo ·
C. Park

Department of Materials Science and Engineering,
Seoul National University, Seoul 151-744, Korea

W. Jo
Institute of Materials Science, Technische Universität
Darmstadt, 64287 Darmstadt, Germany

S.-M. Jeong
Korea Institute of Ceramic Engineering and Technology,
Seoul 153-801, Korea

J.-S. Kim
Korea Institute of Science and Technology,
Seoul 136-791, Korea

C. Park (✉)
Research Institute of Advanced Materials,
Seoul National University, Seoul 151-744, Korea
e-mail: pchan@snu.ac.kr

Introduction

Since the discovery of large thermoelectricity in Na_xCoO_2 [1], much attention has been paid to layer-structured cobaltite materials. Some of the advantages in using cobaltites for thermoelectric applications are their cost-effectiveness owing to the relatively cheap prices of the constituting elements, the environmentally friendly nature of the individual elements, and the chemical stability over a wide range of temperatures from room temperature up to 1000 K [2–5]. However, their low conversion efficiency is often considered as a major drawback. To overcome this, there have been a number of research activities worldwide [3–16]. Most research suggests that one of the simplest solutions is to induce a high-quality texture in the material. The rationale is based on the fact that the $\text{Ca}_3\text{Co}_4\text{O}_9$ (Ca349) cobaltite is a misfit-layered oxide, where two distinctive layers stack alternately on top of each other along the *c*-axis, and thus possesses strongly anisotropic functional properties [17]. For example, it was shown that the electrical resistivity is significantly high along the *c*-axis, because one of the two constituting layers is highly conducting while the other is insulating [17–19]. This strongly suggests that, by inducing a preferred *c*-axis orientation even in a polycrystalline form, one can enhance the electrical conductivity of the materials significantly along the planar directions perpendicular to the texture direction. As noted, the efficiency of energy conversion is described by the so-called dimensionless figure of merit (*ZT*):

$$ZT = \frac{S^2 T}{\kappa \rho}, \quad (1)$$

where *S*, *ρ*, *κ*, and *T* are Seebeck coefficient, electrical resistivity, thermal conductivity, and absolute temperature,

respectively. Equation 1 clearly states that to increase the energy conversion efficiency by the thermoelectric effect, the materials of choice should have as large a Seebeck coefficient and electrical conductivity as possible, while the thermal conductivity should be kept as small as possible. Here, the Seebeck coefficient is closely related to the charge carrier density of the given material, and thus is more or less constant as long as the chemistry, i.e. the composition, is fixed. This is especially true for the Ca349 cobaltite of the current discussion [4]. It follows that a further enhancement and consequent optimization of the thermoelectric properties of a given material depends solely on how to optimize the electrical and thermal conductivities.

In fact, this idea was clearly demonstrated with samples textured by the magnetic alignment technique [9], the reactive templated grain growth technique [8], and single-crystal composite method [15]. However, this in turn proves that making the material of practical importance is extremely challenging. Because the salient properties of the material are guaranteed only when the material is well-textured, the processing of the material requires a high level of complexity, and consequently the processing cost increases sharply. Therefore, a key technological issue to be addressed is how to simplify the processing route to provide a high level of texturing. Here we present a new technique that is simple but highly effective in inducing a high degree of texture in an oxide thermoelectric Ca349. Disk-shaped sheets (~ 0.5 mm thick) of Ca349 fabricated with a uniaxial pressure were stacked together and spark plasma sintered. The effectiveness of the developed technique is evaluated and discussed in terms of the microstructure and the relevant functional properties.

Experimental procedures

$\text{Ca}_3\text{Co}_4\text{O}_9$ (will be referred to as Ca349 hereafter) powders were prepared by a conventional solid-state reaction method. The starting powders of reagent grade CaCO_3 and Co_3O_4 (purity level >99.9%) were weighed according to the stoichiometric formula. The weighed powder was ball-milled in ethanol using zirconia grinding media for 24 h. The dried powder was calcined at 1153 K for 24 h in an oxygen atmosphere two times. A sheet of Ca349 ~ 0.5 mm thick was prepared by a uniaxial pressure of ~ 40 MPa with ~ 0.07 g of powder (Fig. 1a). Then, disk-shaped specimens with 10 mm diameters were cut out of the sheet to be fitted into a carbon die for a spark plasma sintering (SPS) apparatus. Fifteen disk-shaped sheets were stacked together and sintered under a 100 mTorr vacuum at 1173 K for 10 min under a uniaxial pressure of ~ 40 MPa (Fig. 1b). The thicknesses of the sintered specimens were

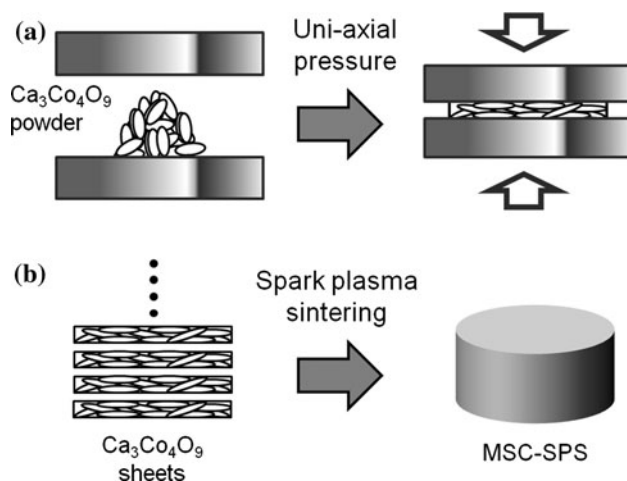


Fig. 1 The schematic explaining the experimental procedures of **a** preparing Ca349 sheets and **b** sintering process using stacked sheets

about 3 mm. After sintering, a re-oxidation process was carried out at 1153 K for 24 h in a flowing oxygen atmosphere. To properly evaluate the effectiveness of the currently developed technique (will be denoted as the multisheet cofiring (MSC) technique hereafter), another batch of specimens were produced via the conventional SPS sintering technique to act as references.

A diffractometer (X'pert Pro, PANalytical, Almelo, Netherlands) equipped with a monochromator generating line-focused $\text{Cu K}\alpha_1$ radiation and a point detector filled with Xe gas was used for all the X-ray diffraction (XRD) studies. The phase evolutions of both calcined powder and sintered samples were monitored in a θ - 2θ mode. To evaluate the degree of (00l) texture, the (002) reflection was chosen and fine-scanned as a function of χ -tilt angles with a step size of 10° . Because the intensity decreases sharply as χ increases due to beam defocusing, two consecutive scans were performed as follows to obtain a complete set of diffraction profiles over the range of $\chi = 0^\circ$ to 90° . First, we installed the specimens in a way that the scattering vector was parallel to the direction of the stress applied during sintering. Note that this orientation will be referred to as $\chi = 0^\circ$ throughout the text. Second, the (002) reflection was recorded by a θ - 2θ scan with the χ angle increasing clockwise up to 40° . After that, the sample stage was brought back to the initial position, and the specimens were unloaded and then flipped 90° clockwise so that the scattering vector was perpendicular to the direction of the applied stress. Here again, for our reference, this orientation will be referred to as $\chi = 90^\circ$ hereafter. Finally, the (002) reflection was collected with the identical procedure but this time the χ angle was changed counterclockwise up to 40° . Two separately collected spectra were then combined together to present the complete structural information of the out-of-plane space. In

the meantime, the same procedure was applied to a randomly oriented CeO_2 ceramic of the same dimensions as the tested specimens to remove measurement errors. All the collected reflections were characterized by fitting the individual reflections with the Voigt shape profile function using a peak fitting module embedded in the commercial software Origin (Originlab, Inc., ver. 7.5).

The morphology of the calcined powder and the microstructures of the sintered bulk samples were investigated by scanning electron microscopy (JSM-6360, JEOL, Tokyo, Japan). To properly assess the microstructural evidence for the texture development, polished and chemically etched cross-sectional surfaces parallel to the direction of the pressure applied during sintering were used.

Bar-type samples ($2.5 \times 2.5 \times 10 \text{ mm}^3$) were prepared to measure the electrical conductivity and the Seebeck coefficient. The electrical conductivity was measured by the 4-point probe method in the temperature range of 573–973 K. To assess the Seebeck coefficient, two K-type thermocouple junctions were attached on both ends of the specimens, and then various uniform temperature gradients with a maximum of 9 K ($\Delta T = 0\text{--}9 \text{ K}$) throughout the sample was induced by heating up one end of the sample using a micro-heater placed close to but not in contact with the samples. The electromotive force (EMF) generated by the induced temperature gradient was measured using the signals from a K-type alumel thermocouple via a nanovoltmeter (2182A, Keithley, Cleveland, USA). The Seebeck coefficient value was calculated from the slope of the ΔT versus EMF plot, and then this value was corrected with the Seebeck coefficient of the alumel wire. The thermal conductivity was determined from the thermal diffusivity (LFA457, NETZSCH, Selb, Germany) and the specific heat capacity (DSC404C, NETZSCH, Selb, Germany), which were measured by a laser flash technique.

Results

Figure 2 shows the morphology of the calcined Ca349 powder, as prepared by a solid-state reaction method. Particles with a very thin disk shape can be observed, which is consistent with the literature [3, 16, 19]. The morphology of the particles implies that not only the electrical properties, but also the surface energy of the material, are strongly anisotropic [20]. The average diameter of the disk-shaped particle is about 3 μm , which is about 10 times larger than the thickness. Consequently, the disk-shaped particle can be mechanically aligned by applying uni-axial pressure.

The XRD profile of the calcined powder is presented in Fig. 3a. In spite of the adopted double-calcination

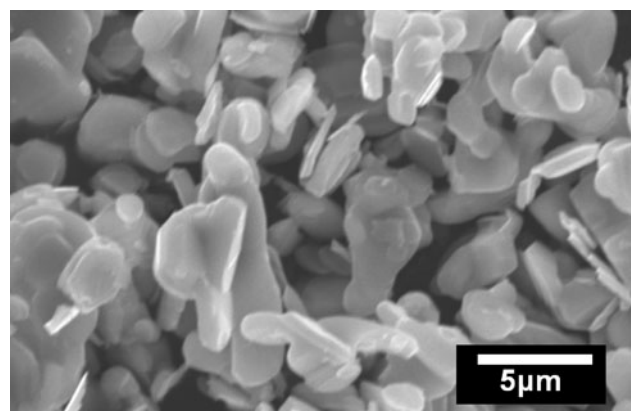


Fig. 2 SEM image of the Ca349 calcined powder

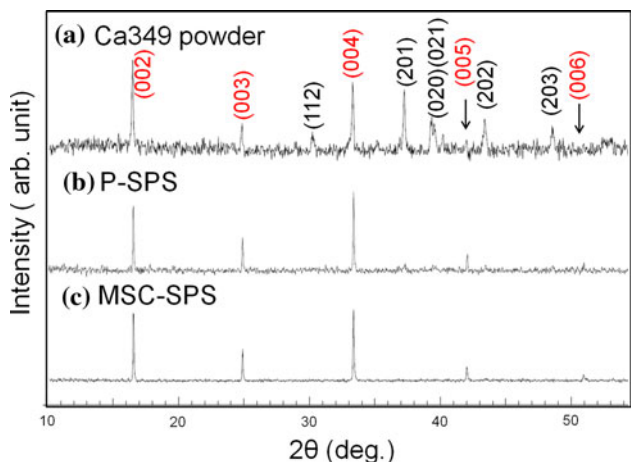


Fig. 3 (Color online) XRD profiles of sintered bulk specimens in comparison with XRD profile of the calcined powder

procedure, it is observed that the formation of the desired phase is not completed and a small trace of unreacted remnants from the starting materials remained, as reflected in the background. These remnants, however, were observed to be completely converted into the desired phase after the sintering process, as shown in Fig. 3b, c. Here, MSC-SPS and P-SPS refers to the specimens produced by the MSC combined with the SPS technique and those produced by the conventional SPS technique applied to the calcined powder, respectively. It is interesting to note that the intensity of the reflections with indices other than $(00l)$ decreases significantly, which indicates the appearance of the preferred orientation along $(00l)$, not only in the MSC-SPS but also in the P-SPS specimens.

Results from the χ -tilt scan on the (002) reflection from the MSC-SPS and P-SPS specimens for selected χ angles are presented, respectively, in Fig. 4a, b to show how the reflection profile evolves with the χ angle. Each profile was fit with the Voigt shape profile function until the 95% confidence interval for each fit was reached. It is noted that,

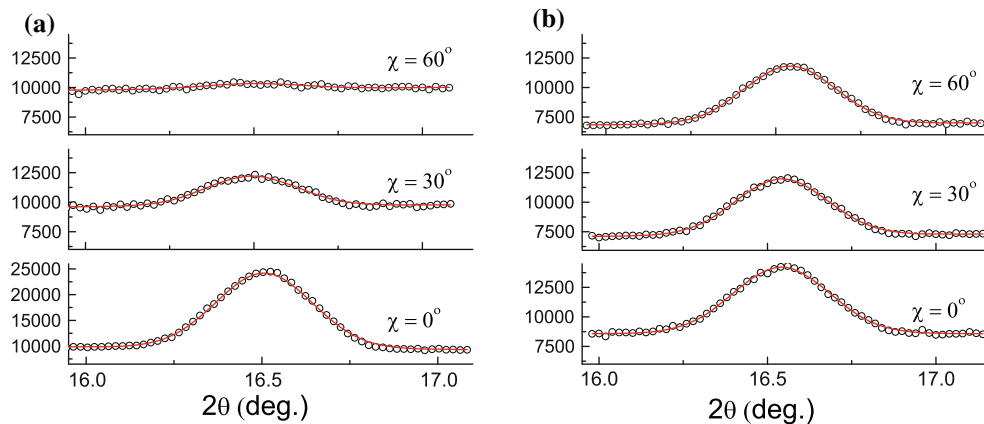


Fig. 4 (Color online) Experimentally obtained profiles (*open circle*) of the (002) reflection from **a** MSC-SPS and **b** P-SPS specimens for the selected χ angles. The obtained reflections are superimposed with a profile fitted by the Voigt function (*solid lines*)

in the case of the MSC-SPS specimen, the peak intensity of the (002) reflection decreases sharply as the χ angle increases, which implies a significant development of texture along the direction where $\chi = 0^\circ$. It was observed that the peak intensity of the (002) reflection relative to that of the background drops exponentially from $\sim 250\%$ at $\chi = 0^\circ$ to $\sim 125\%$ at $\chi = 30^\circ$, and then the intensity asymptotically approaches the background level. In fact, above $\chi = \sim 60^\circ$, the presence of the peak is hardly discernable from the background. In contrast, the peak intensity of the P-SPS specimen stays practically constant even up to $\chi = \sim 60^\circ$, as seen in Fig. 4b.

Polished cross-sectional SEM images of MSC-SPS and P-SPS specimens are shown in Fig. 5a, b, respectively. Both specimens exhibit very dense and fairly homogeneous microstructures in terms of both the average grain size and its distribution. In addition, little difference in the Archimedes' relative density was observed. A theoretical density of $\sim 98\%$ was measured for both samples. However, a careful inspection of the microstructures reveals that the degree of texture is noticeably different from each other. A much higher degree of *c*-axis preferred orientation is noted

in the MSC-SPS sample than that in the P-SPS sample. It is easy to see that the distribution of the arrows that denote the direction perpendicular to the *c*-axis is fairly consistent with the XRD results shown in Fig. 4.

The featured parameters that define the thermoelectric properties of the materials, such as electrical resistivity, Seebeck coefficient, and thermal conductivity, were measured for both the MSC-SPS and the P-SPS samples at various temperatures in air. The electrical resistivity measured along the direction perpendicular to the applied uniaxial pressure, i.e. roughly perpendicular to the *c*-axis, is presented in Fig. 6a. The resistivity of the MSC-SPS specimen is lower than that of the P-SPS sample for all temperatures examined (573–973 K). The temperature coefficient of resistivity (TCR) was determined by a linear regression with reference to the resistivity value at 627 K. The TCR of the MSC-SPS and the P-SPS were estimated, respectively, as $-0.00049 \pm 0.00003 \text{ K}^{-1}$ and $-0.00048 \pm 0.00003 \text{ K}^{-1}$, which are practically identical. These results clearly indicate that the reduction in the resistivity of MSC-SPS is attributed to the formation of texture. Figure 6b shows the temperature-dependent

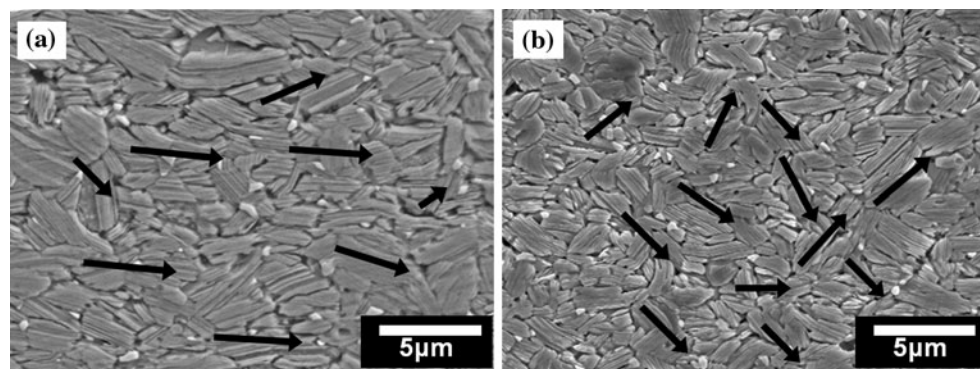
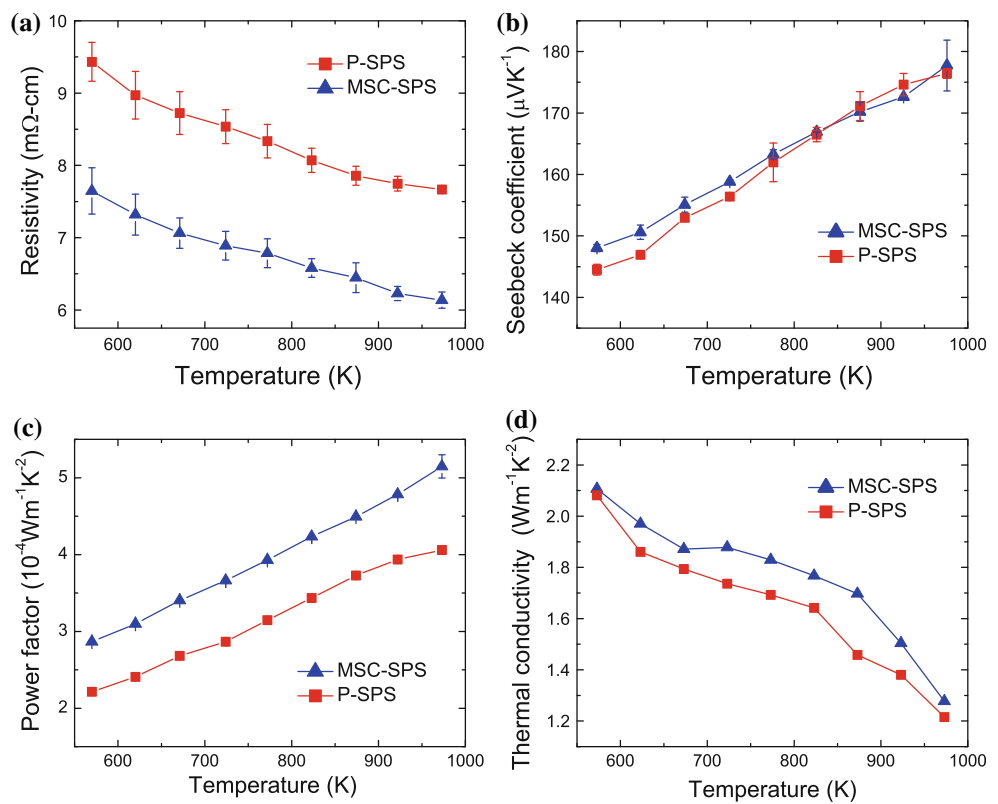


Fig. 5 Polished cross-sectional surface images from **a** MSC-SPS and **b** P-SPS specimens

Fig. 6 (Color online)
 Temperature dependence of
a electrical resistivity ρ ,
b Seebeck coefficient S , **c** power factor, and **d** thermal conductivity for the MSC-SPS and the P-SPS samples



Seebeck coefficients measured along the same direction as the resistivity. The Seebeck coefficient values increase linearly with the temperature from $\sim 146 \mu\text{V/K}$ at 573 K to $\sim 177 \mu\text{V/K}$ at 976 K for both specimens. It was observed that the Seebeck coefficient was nearly the same for both specimens throughout the temperatures scanned (573–973 K).

Kanno et al. [18] have reported that the Seebeck coefficient of the Ca_xCoO_2 system in the direction parallel to the CoO_2 plane (along ab plane) is about $55 \mu\text{V/K}$, which is about two times as large as that along the perpendicular direction at room temperature. In addition, the Seebeck coefficient of a single crystal Ca349 [19] in the direction parallel to the CoO_2 plane, which was $\sim 250 \mu\text{V/K}$ at 1000 K, was higher than those of the polycrystalline bulks and thin films. These results strongly indicate that the Seebeck coefficient of the Ca349 system might exhibit a significant anisotropy as a function of crystallographic orientation. However, it is noted that the majority of literature reports clearly imply that the difference in the Seebeck coefficient as a function of crystallographic orientation should be, if ever, very small in the case of bulk ceramics. For example, most reported Seebeck coefficients are in the range of 175 – $185 \mu\text{V/K}$ at 1000 K regardless of the degree of texture as shown in textured bulks [3, 9, 15]. Given the fact that the reason the anisotropy in the Seebeck coefficient is not evident in the bulk materials is not

clarified in the literature and providing an answer is beyond the scope of the current study, we take our experimental results as they are for the forthcoming discussion.

From the electrical resistivity (ρ) and Seebeck coefficient (S) data, the power factors for both samples, $S^2\rho^{-1}$, are calculated and presented in Fig. 6c. As expected from the resistivity data shown in Fig. 6a, the power factor of the MSC-SPS sample is distinctively larger than that of the P-SPS sample for all temperatures examined (573–973 K). For example, the power factor of the MSC-SPS sample is estimated to be $\sim 5.2 \times 10^{-4} \text{ W m}^{-1} \text{ K}^{-2}$ at 973 K, which is $\sim 20\%$ larger than that of the P-SPS sample.

To assess the dimensionless figure of merit (ZT) of the currently developed materials, the thermal conductivity was measured over the same temperature range as that for the other parameters, as shown in Fig. 6d. In principle, the thermal conductivity should be measured along the same direction as the other parameters for a proper evaluation, but, due to the geometrical constraints enforced by the currently adopted laser flashing technique, the thermal conductivity was measured parallel to the stress applied during SPS (κ_c).

The thermal conductivity values of the MSC-SPS samples were slightly higher than those of the P-SPS samples in the whole range of temperatures. This means that the thermal conductivity is anisotropic along a different crystallographic orientation. Moon et al. [21] and

Itahara et al. [22] reported that the anisotropy ratio (κ_{ab}/κ_c) of the textured Ca349 bulk was about 2.2 and 3, respectively. In this study, the κ_{ab} value needed to calculate ZT was estimated from the measured κ_c with the reported anisotropy ratios. The calculated ZT values of the MSC–SPS samples were 0.18 and 0.13 at 973 K when κ_{ab}/κ_c ratios of 2.2 and 3 were used, respectively.

Discussion

In general, the full description of the texture information for a given system is available from an orientation distribution function (ODF), which defines the density of each possible crystallographic orientation, i.e. poles, with reference to the density of each pole in a randomly oriented specimen. However, a complete construction of pole figures based on the XRD technique is rather impractical, since it typically requires a large number of measurements [23]. In fact, Guilmeau et al. [24] showed that due to a significant defocusing effect of the X-ray beam at $\chi > 60^\circ$, a reliable and successful construction of the pole figures and consequent proper texture analysis is only feasible by neutron diffraction with a curved position-sensitive detector. It follows that the evaluation of the Lotgering factor is often used as an alternative. In fact, it is proposed as a fairly good approximation for evaluating the out-of-plane orientations, i.e. the degree of texture [25]. However, the use of the Lotgering method yields little information on the texture development in the currently studied system because the intensity of the non-(00l) reflections is too small to signify the difference in the texture level between the MSC–SPS and P-SPS samples. In fact, the Lotgering factor calculated for both MSC–SPS and P-SPS samples was similar and almost equal to ~ 1 . Alternatively, therefore, we performed θ - 2θ XRD scans on the (002) reflections as a function of the χ -tilting angle from 0 to 90° with 10° steps to monitor the changes in the population of the (002) poles (see the examples of the collected reflections in Fig. 4).

For all the (002) reflections collected at each χ angle, a single peak-fitting scheme was applied with a 95% confidence band to assess the integrated intensity (I_χ). It is commonly known that, to properly compare the evaluated integrated intensities from each χ angle, a post-processing on the observed intensity is needed to diminish the errors originating from the defocusing of the beam taking place during the χ -tilt scan. This can be done by using a correction factor as follows:

$$I_\chi^{\text{corr}} = \eta(\chi) \cdot I_\chi \quad (2)$$

Here, the correction factor $\eta(\chi)$ should only be dependent on the magnitude of χ . A straightforward way

to determine $\eta(\chi)$ is to perform an additional χ -tilt scan on a texture-free specimen with identical dimensions and chemistry as the specimen in the test. All the other procedures should also be kept identical for both specimens. Then, the correction factor is simply given as $\eta(\chi) = I_{\chi=0^\circ}^{\text{rand}} / I_\chi^{\text{rand}}$, where the superscript rand refers to the randomly orientated specimen. However, a direct application of this method to the current investigation faces a serious problem. Due to the platelet morphology of the starting powder with a high aspect ratio, bulk specimens with truly random orientations are practically impossible to produce. In this investigation, therefore, a CeO₂ ceramic of random orientation carefully tailored to have the same dimension as the Ca349 samples was used instead. To increase the statistical reliability, the (110) reflection, the intensity of which is the strongest, was scanned as a function of χ . Here, the correction factor is given as

$$\eta(\chi) = I_{\chi=0^\circ}^{\text{CeO}_2(110)} / I_\chi^{\text{CeO}_2(110)} \quad (3)$$

The previously calculated integrated intensities from the profile-fitting were then corrected using Eqs. 2 and 3. From these corrected intensities, the relative population of poles (RPP) was evaluated. (200) poles over the χ space were calculated by normalizing the corrected intensities over the total density of the (002) poles based on the following relation:

$$I_\chi^{\text{RPP}} = \frac{I_\chi^{\text{corr}}}{\int_0^{\pi/2} I_\chi^{\text{corr}} d\chi}, \quad (4)$$

where I_χ^{RPP} refers to the relative population of poles at angle χ . Then, the RPP for the completely randomly oriented specimen is given by the averaged RPP values over the entire χ -space as follows:

$$\frac{\int_0^{\pi/2} I_\chi^{\text{corr}} d\chi}{\pi/2} \quad (5)$$

The distribution of RPP of the (002) pole for the specimens prepared both from MSC–SPS and P-SPS is presented in Fig. 7. The dotted line denotes the averaged RPP value representing the randomly oriented specimen given by Eq. 5. A clear distinction in the level of texture between the MSC–SPS and P-SPS specimens is discerned from the distribution profile of the calculated RPP values. It is interesting to note that, although the level of texture is definitively higher in the MSC–SPS specimen, the intercept between the RPP distribution profile and the reference value denoting the random orientation remains the same for both specimens. On the other hand, it is also noted that the RPP values in the MSC–SPS specimen tend to increase when $\chi > 60^\circ$. This abnormality implies that there should be

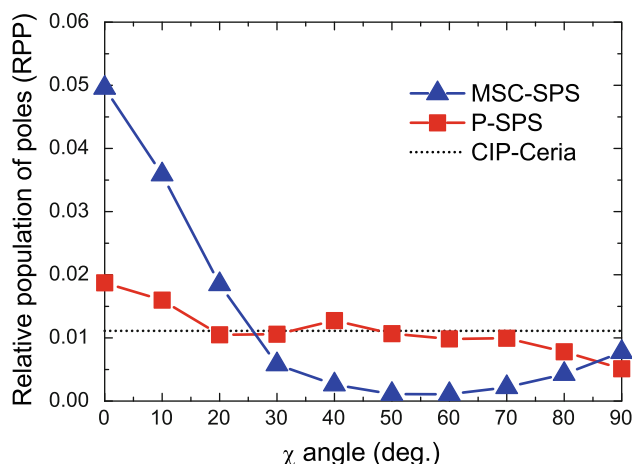


Fig. 7 (Color online) The distribution of the relative density of the (002) poles with respect to the χ angle

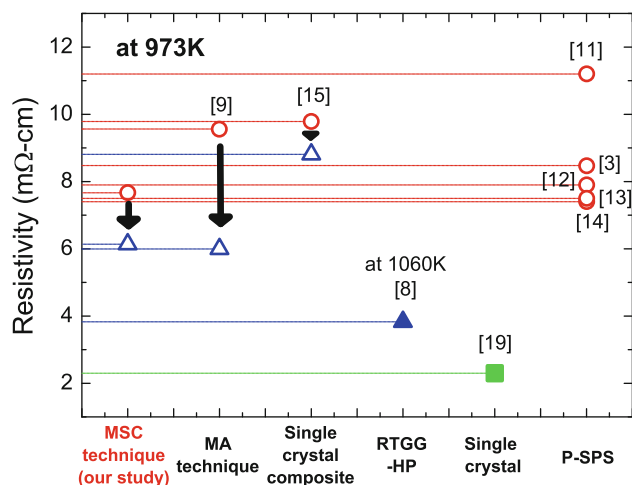


Fig. 8 (Color online) Comparison of the resistivity values from various processing methods. Open circles and closed squares refer to those from the P-SPS samples and single crystal samples, respectively

a critical aspect ratio for the starting powder for the current method to effectively induce texture. This idea is supported by the SEM image presented in Fig. 5 which shows the presence of near-vertically aligned grains with a small aspect ratio.

On the other hand, to assess the effectiveness of the MSC-SPS method introduced in this study, the resistivity values of the specimens produced by various methods in the literature are compared with the results of the current study (Fig. 8). The resistivity as a featured property is chosen because it is the most sensitive to the degree of texture as revealed in the current study (see Fig. 6), and it is relatively free from artifacts during measurement. Although there is a notable fluctuation in the resistivity values of the specimens produced even by the same processing method, i.e. the P-SPS technique, the resistivity achievable by the conventional SPS technique can

be said to be $\sim 7.5 \text{ m}\Omega \text{ cm}$ once the specimen is properly produced. The source of the fluctuation is not clear because the required information, such as the degree of texture as well as the average grain size and its distribution, for a proper comparison is mostly missing in the literature [3, 8, 9, 11–15, 19]. Nevertheless, the factors affecting the resistivity can be inferred from the data presented in Fig. 8. Ignoring the extremely inconsistent data reported in [11], one can grasp a clear idea that the resistivity decreases as the degree of texture increases. In fact, the level of texture induced by the combined technique of the reactive template grain growth (RTGG) and hot pressing (HP) was demonstrated to be extremely high, which explains the significant decrease of resistivity compared with other methods. However, the discrepancy in the resistivity value from that of a single crystal is still notably high. This implies that the resistivity of grain boundaries also plays an important role in determining the overall resistivity of the material.

Summary and conclusions

A highly textured $\text{Ca}_3\text{Co}_4\text{O}_9$ (Ca349) thermoelectric ceramic was manufactured by a simple and economical processing method named as a multisheet cofiring technique. The effectiveness of texturization by the currently developed method was verified both by X-ray diffraction and scanning electron microscopy. The evaluation of the featured thermoelectric properties, such as electrical resistivity, Seebeck coefficient, and thermal conductivity, suggested that the effect of the degree of texture on the enhancement of thermoelectric properties of Ca349 ceramics is mainly attributed to the reduced electrical resistivity. Thus, it was proposed that a key to optimizing the thermoelectric properties of Ca349 ceramics is to induce as high a texture as possible as well as to reduce the electrical resistivity of the grain boundary. In addition, the relative population of poles (RPP) concept was introduced as a relatively easy and effective way to evaluate the degree of texture.

Acknowledgements This work was supported by the Mid-career Researcher Program of NRF/MEST (2010-0000463) in association with the Converging Research Center Program through the Ministry of Education, Science and Technology (2009-0093723) and the Core Technology of Materials Research and Development Program of the Korea Ministry of Intelligence and Economy (K00060071-55512).

References

- Fujita K, Mochida T, Nakamura K (2001) Jpn J Appl Phys 40(7):4644
- Koumoto K, Terasaki I, Funahashi R (2006) MRS Bull 31(3):206

3. Liu YH, Lin YH, Shi Z, Nan CW, Shen ZJ (2005) *J Am Ceram Soc* 88(5):1337
4. Sugiura K, Ohta H, Nomura K, Hirano M, Hosono H, Koumoto K (2006) *Appl Phys Lett* 89(3):032111
5. Shen JJ, Liu XX, Zhu TJ, Zhao XB (2009) *J Mater Sci* 44(7):1889. doi:[10.1007/s10853-009-3279-0](https://doi.org/10.1007/s10853-009-3279-0)
6. Diez JC, Guilmeau E, Madre MA, Marinel S, Lemonnier S, Sotelo A (2009) *Solid State Ionics* 180(11–13):827
7. Son JY, Shin YH, Park CS (2008) *J Appl Phys* 104(3):033538
8. Guilmeau E, Itahara H, Tani T, Chateigner D, Grebille D (2005) *J Appl Phys* 97(6):064902
9. Zhou YQ, Matsubara I, Horii S, Takeuchi T, Funahashi R, Shikano M, Shimoyama J, Kishio K, Shin W, Izu N, Murayama N (2003) *J Appl Phys* 93(5):2653
10. Mikami M, Guilmeau E, Funahashi R, Chong KJ, Chateigner D (2005) *J Mater Res* 20(9):2491
11. Liu HQ, Wang FP, Liu F, Song Y, Jiang ZH (2006) *J Mater Sci Mater Electron* 17(7):525
12. Liu HQ, Zhao XB, Zhu TJ, Song Y, Wang FP (2009) *Curr Appl Phys* 9(2):409
13. Zhang YF, Zhang JX (2008) *J Mater Process Technol* 208(1–3):70
14. Wang DL, Chen LD, Wang Q, Li JG (2004) *J Alloy Compd* 376(1–2):58
15. Guilmeau E, Funahashi R, Mikami M, Chong K, Chateigner D (2004) *Appl Phys Lett* 85(9):1490
16. Prevel M, Lemonnier S, Klein Y, Hébert S, Chateigner D, Ouladdiaf B, Noudem JG (2005) *J Appl Phys* 98(9):093706
17. Masset AC, Michel C, Maignan A, Hervieu M, Toulemonde O, Studer F, Raveau B, Hejtmanek J (2000) *Phys Rev B* 62(1):166
18. Kanno T, Yotsuhashi S, Adachi H (2004) *Appl Phys Lett* 85(5):739
19. Shikano M, Funahashi R (2003) *Appl Phys Lett* 82(12):1851
20. Jo W, Kim DY, Hwang NM (2006) *J Am Ceram Soc* 89(8):2369
21. Moon JW, Nagahama D, Masuda Y, Seo WS, Koumoto K (2001) *J Ceram Soc Jpn* 109(8):647
22. Itahara H, Tani T (2004) *R&D Rev Toyota CRDL* 39(1):63
23. Jones JL, Iverson BJ, Bowman KJ (2007) *J Am Ceram Soc* 90(8):2297
24. Guilmeau E, Chateigner D, Noudem J, Funahashi R, Horii S, Ouladdiaf B (2005) *J Appl Crystallogr* 38:199
25. Lotgering FK (1959) *J Inorg Nucl Chem* 9(2):113